DOI: 10.24930/2500-302X-2025-25-1-44-60

Investigating the Structural Geology Control of the Opak Fault on the Semilir Formation in Yogyakarta, Indonesia

Ardhan Farisan[1], Nanda Ajeng Nurwantari[2], Fadlin[3], Puguh Dwi Raharjo[1], Eko Puswanto[1], Kristiawan Widiyanto[1], Dimas Aryo Wibowo[1]

[1]Research Centre for Geological Resource, National Research and Innovation Agency, Bandung, Indonesia, e-mail: ardh005@brin.go.id
[2]Geological Engineering Department, Faculty of Mineral Technology, University of Pembangunan Nasional Veteran Yogyakarta, Indonesia
[3]Geological Engineering Department, University of Jenderal Sudirman Purwokerto, Indonesia

Поступила в редакцию 22.03.2024, принята к печати 01.05.2024

Research subject. The hill morphology formed in the study area, which is part of the Semilir Formation, is suspected to be a product of Opak fault reactivation. Further investigation is needed to substantiate this claim. *Aim.* To investigate the characteristics of the Opak Fault in the Semilir Formation. The study area is a red zone, which is an area damaged by the 2006 Opak Fault earthquake. *Materials and Methods.* This study was interpreted through integrated data that combined the Digital Elevation Model (DEM) from DEMNAS (Indonesian National Digital Elevation Model), the Digital Outcrop Model (DOM), and extensive field observations. The methodology employed involves investigating DOM interpretation combined with field surveys and morphotectonic methods. *Results*. We have identified the study area as divided into two segments: the northern and southern segments. The characterization of these segments is based on the differences in the alignment of landforms associated with the general direction of the hills and analysis from rosette diagrams. In the northern region, elongated hills are oriented in the NE-SW direction, whereas in the south, they exhibit an N-S block lineation. Field observations reveal the presence of a high-angle fault at observation point A **(Fig. 6a)**, indicating reactivation, and a reverse fault at observation point D1 **(Fig. 6b)**. The rosette diagram results indicate a compression direction of NW-SE in the northern segment and N-S in the southern segment. *Conclusions*. Integrating UAV photogrammetry and Digital Elevation Model (DEM) data has significantly enhanced our understanding of the geological structures within the Semilir Formation in the Opak Fault Zone. The analysis identifies the study area as a reactivation zone of the Opak fault, indicated by the presence of high-angle reverse faults. This reactivation zone and the landscape morphology consisting of hills are interpreted as a zone of destruction resulting from Opak fault movement, previously identified as a sinistral strike-slip fault.

Keywords: *Digital Elevation Model, Digital Outcrop Model, Morphotectonic, Opak Fault, Semilir Formation*

Acknowledgements

This research is an independent study supported by co-authors in data collection. The author would like to thank the Research Center for Geological Resources, National Research and Innovation Agency Indonesia.

Исследование структурной геологии, контролирующей Опакскую разлому на формации Семилир в Йогякарте, Индонезия

Ардхан Фарисан[1], Нанда Адженг Нурвантари[2], Фадлин[3], Пугух Дви Рахарджо[1], Эко Пусванто[1], Кристиаван Видийанто[1], Димас Арьо Вибово[1]

[1]Научно-исследовательский центр по геологическим ресурсам, Национальное агентство научных исследований и инноваций, Бандунг, Индонезия, e-mail: ardh005@brin.go.id
[2]Кафедра геологического инжиниринга, Факультет минеральных технологий, Университет Ветеранов Национального Развития, Йогякарта, Индонезия
[3]Кафедра геологического инжиниринга, Университет Джендерал Судирман, Пурвокерто, Индонезия

Received 22.03.2024 г., accepted 01.05.2024 г.

Для цитирования: Фарисан А., Нурвантари Н.А., Фадлин, Рахарджо П.Д., Пусванто Э., Видийанто К., Вибово Д.А. (2025) Исследование структурной геологии, контролирующей Опакскую разлому на формации Семилир в Йогякарте, Индонезия. *Литосфера*, **25**(1), 44-60. https://doi.org/10.24930/2500-302X-2025-25-1-44-60. EDN: AGCQHJ

For citation: Farisan A., Nurwantari N.A., Fadlin, Raharjo P.D., Puswanto E., Widiyanto K., Wibowo D.A. (2025) Investigating the Structural Geology Control of the Opak Fault on the Semilir Formation in Yogyakarta, Indonesia. *Lithosphere (Russia)*, **25**(1), 44-60. (In Russ.) https://doi.org/10.24930/2500-302X-2025-25-1-44-60. EDN: AGCQHJ

Тема исследования. Морфология холмов, сформировавшаяся в исследуемой зоне, входящей в состав Формации Семилир, предположительно является результатом реактивации разлома Опак. Для подтверждения этого утверждения требуется дальнейшее исследование. *Цель.* Исследовать характеристики разлома Опак в Формации Семилир. Исследовательская зона – красная зона, пострадавшая от землетрясения, произошедшего в 2006 году из-за разлома Опак. *Материалы и методы.* Исследование проводилось на основе интегрированных данных, включая цифровую модель рельефа (DEM) от DEMNAS (Индонезийская национальная цифровая модель рельефа), цифровую модель разрезов (DOM) и обширные полевые наблюдения. Методика включала анализ интерпретации DOM в сочетании с полевыми обследованиями и методами морфотектоники. *Результаты.* Была выделена зона исследования, разделенная на два сегмента: северный и южный. Характеризация этих сегментов основана на различиях в выравнивании рельефа, связанных с общим направлением холмов, и анализе розеточных диаграмм. В северном регионе элонгированные холмы ориентированы в направлении северо-восток–юго-запад, в то время как на юге они образуют блочную линеацию север–юг. Полевые наблюдения выявили присутствие высокоугольного разлома в точке наблюдения A **(рис. 6a)**, указывающего на реактивацию, а также обратного разлома в точке наблюдения D1 **(рис. 6b)**. Результаты розеточной диаграммы показывают направление компрессии северного сегмента NW-SE и южного сегмента N-S. *Выводы.* Интеграция данных фотограмметрии с использованием БПА и цифровой модели рельефа (DEM) значительно улучшила наше понимание геологических структур в Формации Семилир в Зоне разлома Опак. Анализ показывает, что зона исследования является зоной реактивации разлома Опак, что подтверждается наличием высокоугольных обратных разломов. Эта зона реактивации и морфология ландшафта, состоящая из холмов, интерпретируются как зона разрушения, обусловленная движением разлома Опак, ранее определенного как разлом с левым сдвигом.

Ключевые слова: *цифровая модель рельефа, цифровая модель открытого разреза, морфотектоника, сбой Опак, формация Семиллир*

Благодарности

Это исследование является самостоятельным исследованием, поддержанное соавторами в сборе данных. Автор хотел бы поблагодарить Центр исследований геологических ресурсов Национального агентства исследований и инноваций Индонезии.

INTRODUCTION

The Java Subduction Zone, located south of Java, Indonesia, is an integral component of the Indo-Australia and Sundaland subduction systems. This geological feature serves as an exemplar of orthogonal subduction. Its historical activity extends as far back as the Paleogene period, as documented by Hamilton (1979) and Hall (2012). Based on Metcalfe (2017) in **Fig. 1a**, the convergence rate indicates a range of approximately 5cm/ year. The convergence of oceanic plates results in the creation of a subduction system, which includes the Andaman-Sumatra-Java trench to the West and South and the Philippine Trench to the East (Li et al., 2021). The tectonic activity is associated with the Yogyakarta earthquake that occurred on May 26, 2006. The United States Geological Survey estimated the earthquake's magnitude to be Mw 6.3. (USGS Preliminary Earthquake Report, 2006). Since then, approximately 750 aftershocks have been recorded, with the largest measuring Mw 5.2 (Consultative Group on Indonesia, 2006).

The Opak Fault activity has been considered the major controller of the Yogyakarta earthquake in 2006 (Karnawati et al., 2006; Walter et al., 2008). Opak Active Fault is inferred to be 45 km in length and oriented in a northeast-southwest direction. Specifically, the Opak Fault exhibits a slip rate of 4–6 mm per year, and historical records indicate a maximum magnitude of 6.60 Mw (Abidin et al., 2009a; Abidin et al., 2009b; PUSGEN, 2017). The Opak Fault was initially documented by Rahardjo et al. (1995) in the Geologic map of the Yogyakarta quadrangle, Java, at a 1:100,000 scale, characterized as a normal fault. Most researchers agree that the kinematic of opak fault is a Sinistral Strike-slip (Natawidjaja, 2007; Abidin et al., 2009b; Tsuji et al., 2009; Natawidjaja, 2016). The Opak Fault crosses through the study area along the western escarpment of the Baturagung range. The earthquake damage zone associated with the Opak Fault extends into a densely populated area that runs northeast from the Parangtritis area to the Bantul area and continues northward to the Klaten region (Abidin et al., 2009b).

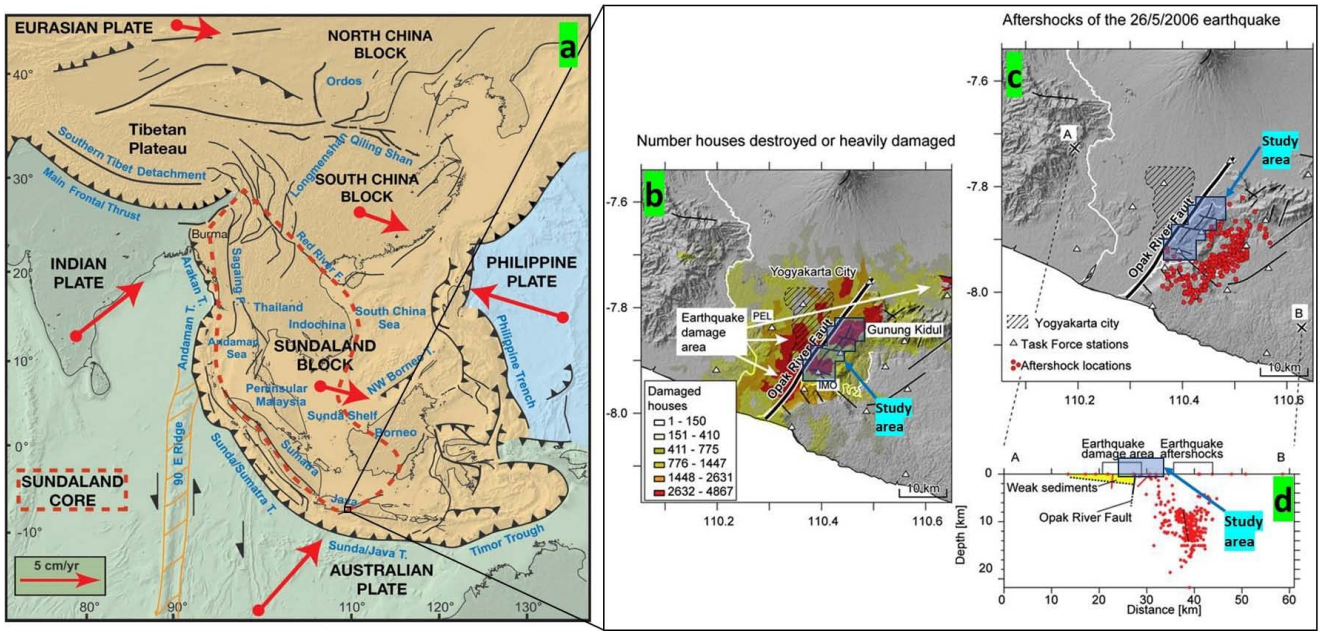

Fig. 1. (a) The tectonic region of Asia with the location of the research area (Metcalfe, 2017); (b) Earthquake damage area following the Opak Fault (Walter et al., 2008); (c) The distribution of aftershocks from the 2006 Yogyakarta earthquake (Walter et al., 2008); A cross-section reveals the presence of an Opak River Fault plane dipping to the west, with earthquake aftershocks located to the east of the Opak River Fault and exhibiting an eastward dip (Walter et al., 2008).

Рис. 1. (a) Тектонический регион Азии с указанием местоположения исследовательской области (Metcalfe, 2017); (b) Зона повреждений от землетрясения вдоль разлома Опак (Walter et al., 2008); (c) Распределение подземных толчков после землетрясения в Йогакарте 2006 года (Walter et al., 2008); На поперечном разрезе видна плоскость разлома реки Опак, наклоненная на запад, с подземными толчками расположенными к востоку от разлома реки Опак и проявляющими восточное наклонение (Walter et al., 2008).

The area of damaged houses along the Opak fault aligns parallel with the straightness of the Opak River, extending from NE-SW (Fig. 1b). The aftershock data (Fig. 1c) indicated that the seismic source was also parallel to the Opak Fault but located about 10–20 kilometres to the east within the mountainous and less densely populated region of Gunung Kidul, in a NE-SW direction (N037°E), and concentrated along-strike within 19 km range and across-strike within 4 km and in the depth 8-15 km (Koulakov et al., 2007; Wagner et al., 2007). Fig. 1d illustrates the earthquake damage area, which is predominantly associated with a northwest-dipping fault located within the relatively soft sediment deposits originating from the Merapi volcano. On the other hand, the aftershocks are distributed to the east, encompassing a range of depths from 0 to 20 kilometers. The geological field study conducted by Walter et al. (2008) showed significant discrepancies when compared to the earthquake aftershock recordings documented by Fukuoka et al. (2006). In the References 2008 To reconcile this difference, Natawidjaja (2016) proposed a hypothesis suggesting that the fault plane likely has an inclination of approximately 50 degrees toward the east.

Yogyakarta is located within a north-south-oriented depression characterized by Quaternary deposits, primarily composed of volcanic materials from the highly active Merapi Volcano. This volcanic activity significantly influences the local geological and morphological features. The depression's formation can be attributed to the subduction process between the Indo-Australian and Eurasian plates, leading to the development of an Oligo-Miocene volcanic arc, which is currently inactive. Yogyakarta City is generally flat, flanked by elevated terrain to the east and west. Along the Yogyakarta Valley's southern coast is a broad, gently sloping beach. The hilly topography of the Southern Mountains predominantly results in steep eastern coasts within the province (Rahardjo et al., 1995).

According to Rahardjo et al. (1995) and Surono et al. (1992) in **Fig. 2**, the stratigraphy consists of Alluvial deposits (Qa; gravel, sand, silt, and clay); Merapi Alluvium (Qa; tuff, sand, ash, and agglomerate); Sambipitu Formation (Tms; tuff, shale, and siltstone); Wonosari Formation (Tmwl; calcarenite limestone, and reef limestone); Nglanggeran Formation (Tmn; volcanic breccia and tuff); and Semilir Formation (Tmse; breccia tuff and clay tuff). The study area is focused on

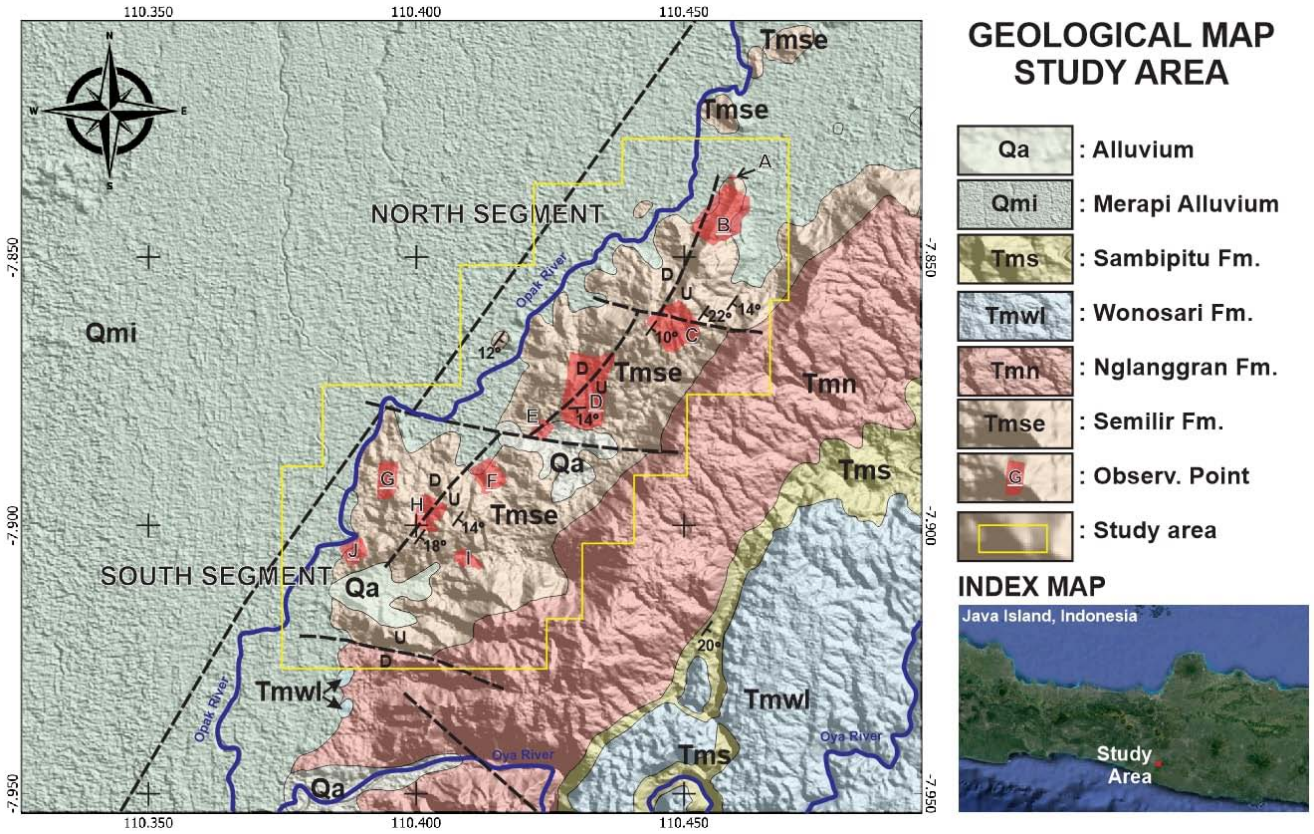

Fig. 2. Regional geological map of the study area with observation point location (Modified from Rahardjo et al., 1995).

Рис. 2. Региональная геологическая карта исследуемой области с указанием местоположения точек наблюдения (Изменено по Rahardjo et al., 1995).

Semilir Formation (Tmse). Semilir Formation was exposed throughout the Southern Mountains and along the southern coast of central Java. The majority of the volcanic materials found in the Semilir Formation are crystal tuff, tuf lapilli, and pumice breccia. Lithic-feldspathic wacke sandstone makes up the lower part of this formation. Lower calcareous foraminifera and nannofossils reveal a marine environment and an early Miocene age/ Burdigalian/ NN3 (Surono, 2008). Andesite breccia and sandstone make up the higher portion. Above are some thin lignite lenses and wood fossils in a few locations. The upper section prominently illustrates the widespread distribution of grain-flow sediments, which has led to the interpretation of terrestrial deposition in this stratum. Radiometric dating of the pumice-breccia within this section revealed two distinct ages, approximately 17.0 ± 0 million years and 16.0 ± 1 million years, respectively, signifying the conclusion of the early Miocene epoch. The brightening of the surroundings near the Semilir Formation suggests a shallow uplift, marking the transition from a shallow sea to a terrestrial environment. Sandstone facies and andesite breccia deposition in this stratum occurred relatively rapidly. Notably, these sandstone facies and andesite breccia signify an increasing trend in volcanism towards the top of the formation (Surono et al., 1992).

The objective of the research is to investigate the characteristics of the Opak Fault in the Semilir Formation. Based on **Fig. 1b**, the study area falls within the red zone, indicating a high incidence of house damage. This prompts the author to question whether this hilly region is the reactivation zone of the Opak Fault and what the geological structure conditions are in this area. The geological features of the Semilir Formation are of specific interest to the study due to their distinct brittle characteristics, which facilitate a clear observation and analysis of the underlying geological structures. The workflow is divided into several steps: (1) Remote sensing analyses using UAV photogrammetry/ Digital Outcrop Model (DOM), Satellite image data (BING, and Google Earth), and DEM (Digital Elevation Model) data; (2) Outcrop study including direct measurement; (3) Morphotectonic analyses; and (4) Geomodeling. Unmanned Aerial Vehicles (UAVs) play a significant role in worldwide geological research. UAV-based photogrammetry is capable of generating statistical and geometrical data, allowing for the dissemination of information regarding fracture/fault characteristics, fold trends, direction, types,

and reconstruction. (Vollgger et al., 2016; Panara et al., 2022). Photogrammetry and remote sensing have advantages as their principal objective for automatically reconstructing geometric models for three-dimensional terrain objects, surfaces, and features from two-dimensional photographs. The 3D models can be effortlessly generated for surface texture and geometric data (Pringle et al., 2004; Hodgetts et al., 2004).

DATA AND METHODS

This study conducted a thorough analysis of fault and lineation sections through a descriptive approach, carefully considering homogeneous segments based on their distinct morphologies and geometries, each potentially representing individual surface rupture lengths. The structural geology was interpreted through an integrated methodology that combined the Digital Outcrop Model (DOM) and extensive field observations. To facilitate this analysis, we utilized Digital Elevation Models (DEM) in conjunction with remote sensing data from Google and BING satellite imagery. Our fault and lineation mapping strategy involved the identification of geomorphological and morphotectonic variations, as well as the strategic selection of field locations, offering valuable opportunities for further in-depth research. By merging these techniques, we aimed to gain a comprehensive understanding of the geological and structural complexities within the study area.

Digital Outcrop Model (DOM)

Geosciences benefit from collecting high-resolution three-dimensional (3D) data at all scales, from hand specimens to landscapes, and numerous techniques are available to handle various scale ranges (McCaffrey et al., 2005; Menegoni et al., 2023; Corradetti et al., 2022; Panara et al., 2022). Unmanned Aerial Vehicle (UAV) photogrammetry has excellent potential for structural geology applications despite technological (e.g., battery life/flight time), natural (e.g., weather), and legal (e.g., flying within visual line of sight) limitations (Manna et al., 2023; Menegoni et al., 2022; Tannant et al., 2017). We could remotely collect an entire brittle and ductile structural dataset, which was then processed, interpreted, and used for 3D implicit modeling, even though traditional structural fieldwork was minimized in this study. One of the challenges we faced was finding reliable sense-of-shear markers from aerial photographs at the working scale of our study, which are essential for the kinematic and dynamic reconstruction of the tectonic past. Human field measurements were required because the high-resolution aerial photographs could not resolve striations on fault planes or slickened lines (Vollgger and Cruden, 2016).

a. Data Acquisition

Due to the complexity of the terrain and sparse cellular connection, most UAV surveys were carried out manually. The photographs were obtained using a combination of strip and convergent capture models, which were employed to mitigate distortion effects, including doming (James and Robson, 2014). A quadcopter of the Unmanned Aerial Vehicle (UAV) type DJI Mavic Air 2 with a consumer GPS/GLONASS satellite system and a 12 to 48-megapixel (maximum) camera was used to carry out the photogrammetric acquisition. The UAV platform and camera's technical specifications are listed in **Table 1**.

b. Data Processing

With GPS-onboard coordinates, all 3392 images within 9 acquisitions were geo-referenced. The photogrammetry 3D Digital Outcrop Model (DOM) was created using The Agisoft Metashape software and the Structure-from-Motion (SfM) technique. Using the software's high accuracy and the pair pre-selection method, which considers the image positions registered by the UAV-GPS, 3392 photos were aligned. The Agisoft Metashape workflow used to produce model data has the following five (5) phases: 1) image matching, bundle adjustment, and creation of a sparse point cloud; 2) creation of a dense point cloud; 3) creation of a mesh; and 4) creation of a texture 5) Orthophotographs generation. The results of orthophotography are quite excellent and suitable for interpretation. Using the UAV's registered onboard photos, the WGS84/EPSG 7030 - UTM49S coordinate system georeferenced the model.

c. Digital Outcrop Model (DOM)

The Digital Outcrop Model (DOM) proves to be well-suited for interpretation due to its evident data processing and clear structural geology depiction (see **Fig. 3**). Specific requirements must be met to validate this interpretation: 1) Adequate Background Data: The research data must be substantiated with information about regional and local geology and insights from previous studies to support model interpretation. Regional geological maps, sourced from Rahardjo et al. (1995), are essential for this purpose. 2) Structural Geology Analysis: Comprehensive analyses and modeling in the field of structural geology are indispensable to this validation process. 3) Model Interpretation:

Table 1. Drone specifications

Таблица 1. Спецификации беспилотного летательного аппарата

Type	**DJI Mavic Air 2**
Total weight	570 g
Camera sensor size	1/2 inch
Camera sensor resolution	48 megapixels
GNSS type	Consumer (standalone)
GNSS accuracy	±1 meter

Fig. 3. Example DOM from observation point G. The DOM shows that structure geology is visible to interpret.

Рис. 3. Пример цифровой модели поверхности (DOM) из точки наблюдения G. DOM показывает, что структурная геология видна и может быть интерпретирована.

Effective model interpretation is crucial for reinforcing the analyses and hypotheses derived from the data. To determine offsets across scarps, we employed UAV-generated DOM by drawing profiles perpendicular to the fault and calculating relative elevation differences.

Digital Outcrop Models (DOM) were developed and interpreted at designated locations denoted as B, C, D, E, F, G, H, I, and J (as illustrated in Fig. 2). The study yielded high-resolution outputs, with the Digital Elevation Model (DEM) exhibiting resolutions ranging from 11.6 to 47.3 cm and the orthomosaic achieving resolutions between 2.21 and 5.91 cm. A comprehensive visual inspection of the 3D DOMs provided compelling validation of the photogrammetric products, aligning effectively with the research objectives. The detailed results of the photogrammetric analysis are presented in Table 2.

Morphotectonic

The structural study is based on recognizing and mapping the main structures on aerial photographs, DEMNAS (Indonesian National Digital Elevation Model), and outcrop study. The DEMNAS was built from several data sources, including IFSAR data (5 m resolution), TERRASAR-X (5m resampling resolution from 5–10 m original resolution), and ALOS PALSAR (11.25 m resolution), by adding mass point data used in making the Indonesian Topography Map. The spatial resolution of DEMNAS is 0.27-arcsecond, using the EGM2008 vertical datum (https://tanahair.indonesia.go.id/demnas).

An essential step in the study was localizing the faults and other tectonic structures, such as the major fault, fracture, or shear zones. The goal of the analysis was to interpret a number of linear indications that could represent tectonic structures. The analysis results were validated by the structural data acquired during the field survey and from the Digital Outcrop Models. To obtain the best results, we extracted tectonic structures from hill-shading from DEMNAS reliefs and overlaid DEM and DOM results extracted from the photogrammetry method.

Workflow

1. Several data and analyses were used during this study:
- UAV photogrammetric acquisition for the development and analysis of DOMs, DEM, and orthoimages.
- Ground Observation: Comprehensive structural geological field surveys.
- Morpho-structural analysis based on DEMNAS data.
- Morpho-structural analysis using satellite imagery sourced from Google Earth and BING.

2. The data processing phase is subdivided into two distinct components:
- Photogrammetry processing encompasses a series of key steps involving handling photogrammetric data. This process includes procedures such as image matching, dense cloud generation, meshed model creation, textured model generation, and orthophoto generation.

Table 2. Photogrammetry Result

Таблица 2. Результаты фотограмметрии

Observation Point	PARAMETER					
	Photo	Dense Cloud (points)	Tiled Model Resolution (cm/ pixels)	DEM Resolution (cm/ pixels)	Orthomosaic Resolution (cm/ pixels)	Area (hectares)
B	675	8.097.600	5.42	43.4	2.21	87.1
C	578	7.214.200	2.21	85.9	2.21	62.64
D	696	8.681.066	5.91	47.3	5.91	115.47
E	126	15.457.080	2.89	11.6	2.89	10.37
F	349	4.170.965	4.36	34.9	4.36	26.76
G	260	29.484.107	3.08	12.3	3.08	18.11
H	350	10.141.284	2.84	22.7	2.84	26.57
I	181	14.149.230	3.60	14.4	3.60	11.26
J	177	22.236.284	3.39	13.6	3.39	17.95

- Geographic Information System (GIS) analyses are employed to conduct comprehensive morphotectonic investigations.

3. The result encompasses several integral components:

- Digital Outcrop Model (DOM): DOM analysis integrates the results of orthophotographs and Digital Elevation Models derived from photogrammetric processing, enhancing the validation of morphotectonic analyses.
- Morphotectonic Map: The development of a morphotectonic map, a fundamental outcome of this study, provides a visual representation of tectonic and structural features.
- Geo-Model Interpretation: In the realm of geomodel interpretation, we delve into the identification of structural geological characteristics, significantly contributing to our comprehensive analysis.

These components collectively form the basis of our results. The findings were rigorously validated and cross-referenced with regional geological data and previous studies to bolster their validity, resulting in strengthened hypotheses and refined analyses for the most robust outcomes. The complete workflow can be seen in **Fig. 4**.

RESULT AND DISCUSSION

Structural Geology Interpretation

The structural Interpretation sub-chapter elaborates a comprehensive analysis of potential indicators for tectonic or structural geological events. To increase confidence in the interpretation of geological structures, we employ an integrated approach that combines the outcomes of the photogrammetric process, namely the tiled model and orthophotograph, with the Digital Elevation Model (DEM). This layer overlay technique offers valuable insights by elucidating distinctions in terms of the height and shape of the object under examination, thereby enhancing the accuracy and robustness of the interpretation.

We partitioned the study area into two distinct segments, specifically the North and South segments. This division is predicated on disparities in morphological formations and is demarcated by prominent fault indications running from west to east, as illustrated in **Fig. 2**. The North Segment encompasses Observation Points A, B, C, D, and E, while the South Segment comprises Observation Points F, G, H, I, and J.

The North Segment is typified by an elongated hill, aligned in a NE-SW direction, resembling the linear orientation of the Opak Fault (as described by Rahardjo et al., 1995). In contrast, the south segment characterized a relatively North-South block lineation.

1. North Segment

a. UAV-based Aerial interpretation

In the interpretation results obtained from Observation point B, as depicted in **Fig. 5a**, we found the main structure as a major fault associated with the lineation of the hills landscape, further defined as F2. This structure is the major one that controls the morphology of the hills and can be associated with the Opak fault, as interpreted by Rahardjo et al. 1995. We interpret this F2 structure as a normal fault. In the observation B in **Fig. 5a**, we identify several minor compression shear structures (Fb1, Fb2, Fb3, Fb4, and Fb5), trending NW-SE, NE-SW, N-S, and W-E, that F2 delimits. These minor structures have developed in association with the F2 fault. Three NW-SE trending structures (Fc1, Fc2, and Fc3) were identified at Observation

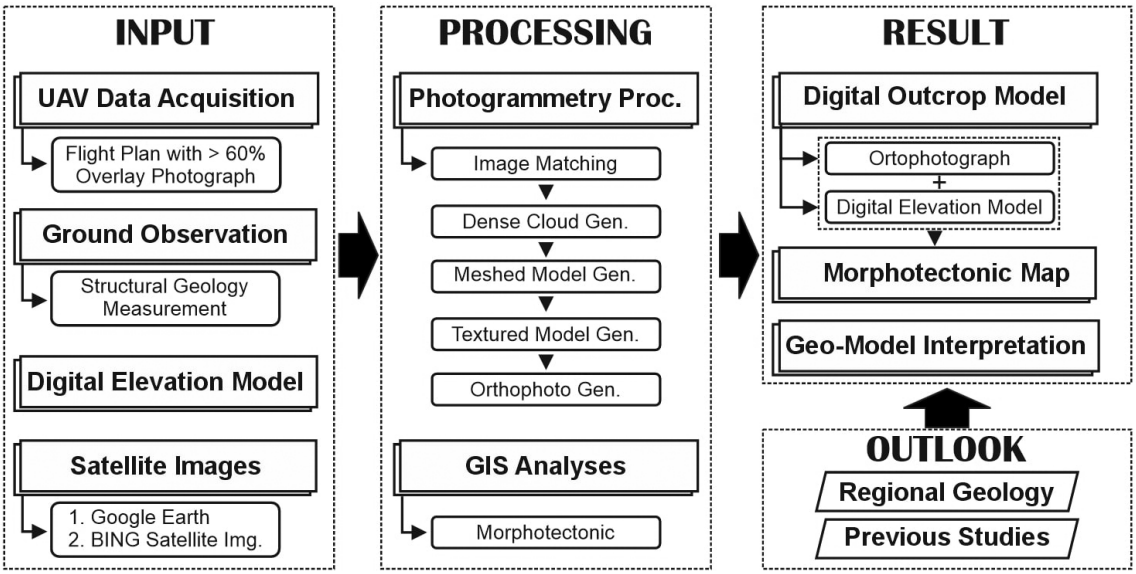

Fig. 4. Schematic workflow followed for this research. Input, processing, and result integration with essential data.

Рис. 4. Схематический ход работы, пройденный в ходе исследования. Ввод, обработка и интеграция результатов с ключевыми данными.

point C in **Fig. 5b**. These structures are oriented perpendicular to the F2 structure, which acts as the controlling factor for the hill's morphology.

Different structural characteristics were observed at Observation points D and E **(Fig. 5c and 5d)**. The major structures at Observation points D and E (Fd3, Fd4, Fd5, Fe1, and Fe2) exhibit an N-S orientation. At Observation point D, three major faults were identified, appearing to be relatively parallel in alignment. The movement of these major faults (Fd3, Fd4, and Fd5) in Observation point D can be indicated by the displacement of the Fd2 as a reverse fault (further detailed in the ground observation sub-chapter). The relative motion of the east block being more northerly than the west block indicates the movement. Based on this evidence, it is proposed that the major fault (Fd3, Fd4, and Fd5) at Observation point D may be characterized as a sinistral strike-slip fault. The author's hypothesis suggests that these strike-slip faults move when the study area undergoes a transpressive phase. At observation point E, two linear features oriented in an N-S direction were identified.

b. Geological Field Survey

The indication of reversal reactivation was found in Observation point A **(Fig. 6a)**, identified as Fa1. Located in the north research area, we found Semilir Formation in the form of tuff and lapilli with a plane of N072°/17° (strike/dip) and a reverse fault with a plane of N096°/75°. A Reverse fault was also found at observation point D1 **(Fig. 6b)** inside of the observation D **(Fig. 5c)**, identified as Fd2, with fault plane of N093^{O}E/64^{O} and Rake of 78°. Reverse faults with high-angle dip intersecting these Semilir formations indicate a compressive tectonic phase. The hypothesis of previous researchers (Pena-Castellnou et al., 2021) is that the study area is controlled by normal faults, which have subsequently undergone reactivation and inversion, transforming into a transpression zone characterized by the presence of both reverse and strike-slip faults.

At Observation point A and D1 **(Fig. 6a and 6b)**, we observed the presence of a high-angle reverse fault, which can be attributed to tectonic inversion. Inversion tectonics is a result of normal faults that frequently reactivate as reverse faults during contraction (Withjack et al., 1995; Beauchamp et al., 1996, 1999; Gomez et al., 2000; Sagir, 2001; Hill et al., 2004; Konstantinovskaya et al., 2007). A normal fault may be reactivated as a high-angle reverse fault and thrust as a low-angle normal fault during compressional inversion (Sibson, 1985; Turner and Williams, 2004) caused by low frictional strength. Analogous and numerical models show that high-angle reversal faults can reactivate due to frictional weakening (Smith et al., 2017).

2. South Segment

Our UAV-based structural analysis in the southern segment highlights significant structural heterogeneity. Observation at point F **(Fig. 7a)** reveals two major NW-SE oriented faults alongside several structures aligned with Riedel shear structures located between these major faults, known as Ff1 and Ff4. Within this fault zone, we identify discrete fragments or blocks separated by

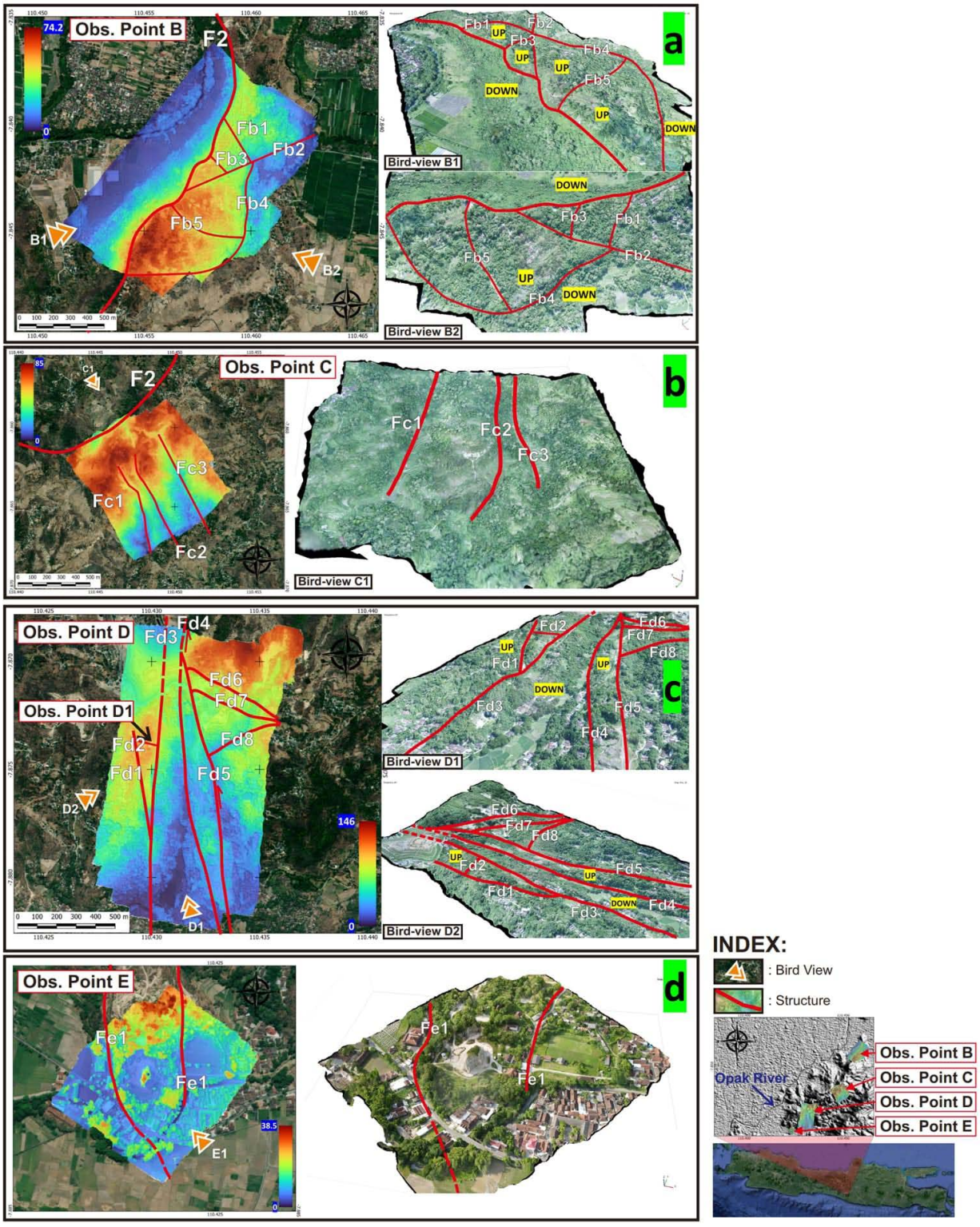

Fig. 5. The result: (a) Obs. point B: major fault (F2) associated with the lineation of the hills landscape and shear; (b) Obs. point C: lineation perpendicular with F2; (c) Obs. point D: the N – S sinistral fault associated with reversal reactivation; (d) Obs. point E: Lineation with N – S trend.

Рис. 5. Результат: (a) Набл. точка B: основной разлом (F2), связанный с геол. линейность холмистого ландшафта и сдвигом; (b) Набл. точка C: геол. линейность перпендикулярна F2; (c) Набл. точка D: N - S левый разлом, связанный с реактивацией реверса; (d) Набл. точка E: геол. линейность с трендом N - S.

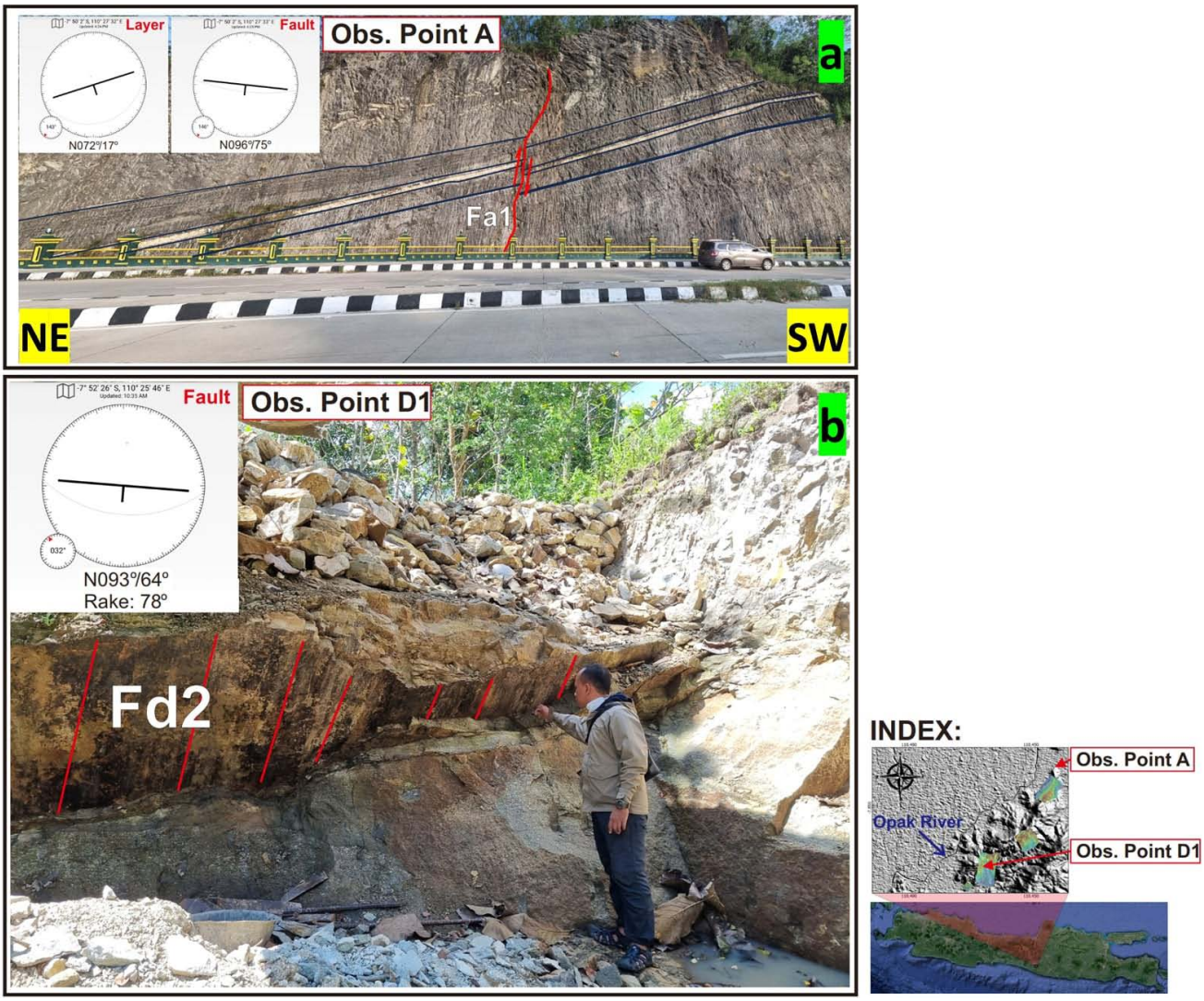

Fig. 6. The result: (a) Obs. point A: High angle fault that indicated reversal reactivation; (b) Obs. point D1: The reverse fault is an indication of reactivation.

Фиг. 6. Результат: (a) Набл. точка A: Высокоугольный разлом, указывающий на реактивацию реверсии; (b) Набл. точка D1: Реверсивный разлом является признаком реактивации.

a network of minor subsidiary faults, which act as secondary structures, further compartmentalizing the region. These fragments move in a direction consistent with the NW orientation of their major faults (Ff1 and Ff2). Notably, the shear zone between the major faults exhibits minor faults oriented in line with Riedel R and R' structures, suggesting that the shared directional movement is due to strike-slip kinematics operating along these major faults (Ff1 and Ff2).

A similar strike-slip movement is also observed at point G. As depicted in **Fig. 7b** the major fault (Fg1 and Fg8) at point G runs nearly perpendicular to the north-south (N-S) axis. Here, we identify en-echelon fractures (Kim et al., 2004) with varying orientations, indicating transpressive features. These minor faults within the transpression fault zone result in duplexing within their major fault, which is a relatively less common occurrence in strike-slip duplexes. This fault-stepping geometry is also observed in sandstone deformation bands (Cruikshank et al., 1991; Fossen and Hesthammer, 1997).

At observation point H, as illustrated in **Fig. 7c** we encounter a distinctive structural lineation oriented to N-S (Fh1 and Fh2), taking on a 'Y' shape predominantly visible on the northern side. Moreover, the eastern flank of this major structure exhibits minor structures with NE-SW and NW-SE trends, referred to as Fh3 and Fh4, respectively.

Observation Point I **(Fig. 7d)** is located along the eastern edge of the southern segment's hills. Similar

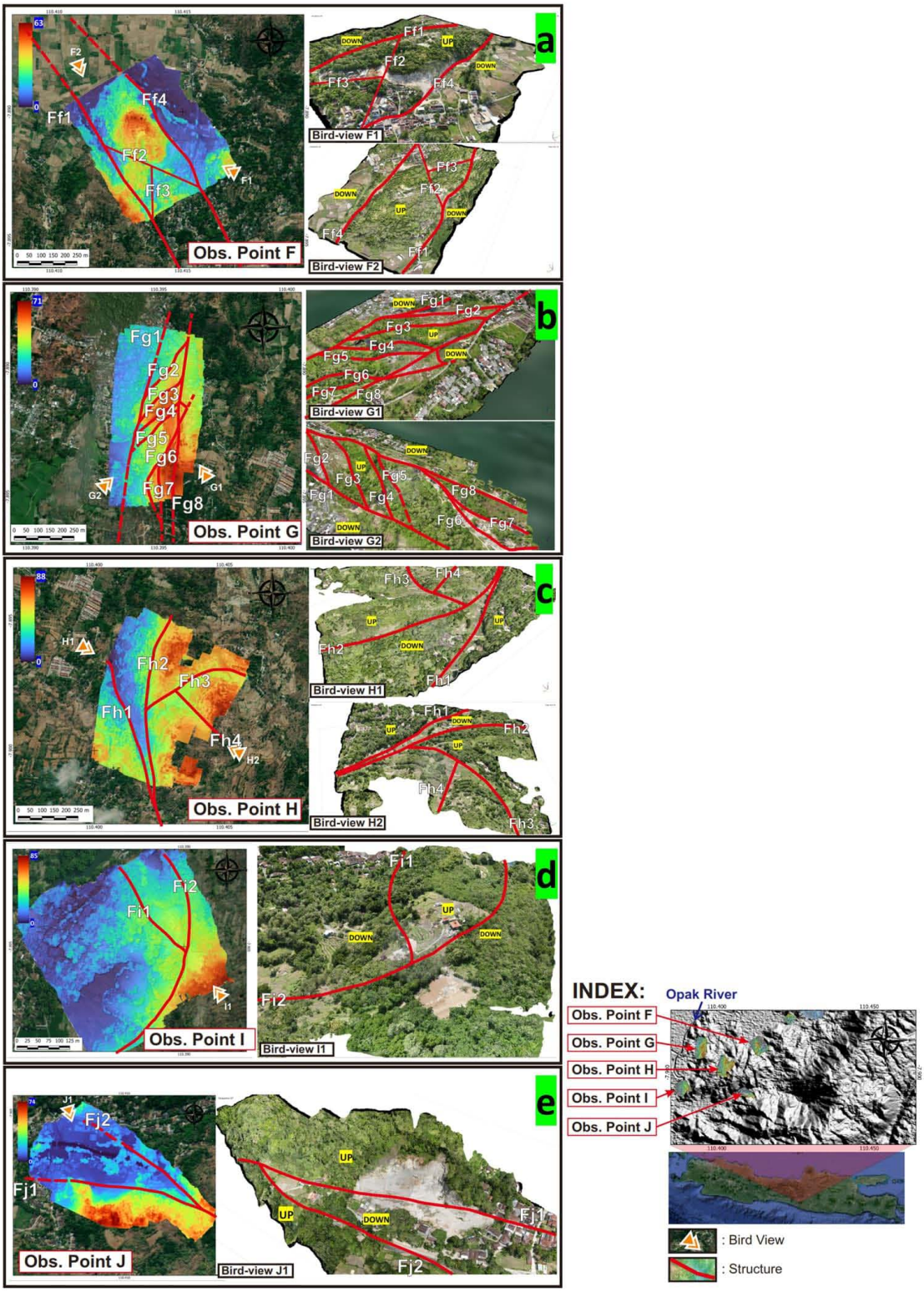

Fig. 7. The result: (a) Obs. point F: Northwest – Southeast trending lineation; (b) Obs. point G: N – S fault associated with shear development; (c) Obs. point H: Lineation trend in the border between hills; (d) Obs. point I: Lineation in the western part of hills; (e) Obs. point J: Lineation in the boundary of southern hills.

Фиг. 7. Результат: Набл. точка F: Линеация с трендом северо-запад – юго-восток; Набл. точка G: N – S разлом, связанный с развитием сдвига; Набл. точка H: Тренд геол. линейность на границе холмов; Набл. точка I: геол. линейность в западной части холмов; Набл. точка J: геол. линейность на границе южных холмов.

to our findings at Observation Point H, the geological structure at Observation Point I resembles a 'Y' shape, with the main axis oriented N-S. Transitioning to the southern part of the South Segment, specifically at Observation Point J **(Fig. 7e)**, we come across a geological feature shaped like a 'Y,' with its major orientation extending from W to E.

Morphotectonic

The research methodology involves the generation of morphotectonic maps through the interpretation of geological structural phenomena. To further validate the geological structures discussed in the previous section, we utilize the results of DOM interpretation. In geodynamically active areas of the world, landforms created by fault-related activities are common. These landforms were uplifted by tectonic processes and further sculpted by geomorphological processes (Keller and Pinter, 1996; Ollier, 1981). Geomorphic landscapes, which are represented by a variety of morphotectonic features, show evidence of surface processes that are adapting to recent bedrock activity. (Stewart and Hancock, 1990, 1994; Schoenbohm et al., 2004; Snyder et al., 2000; Silva et al., 2003)

The northern and southern segments are controlled by major fault lines known as F1 and F5 in the east **(Fig. 8 and 9)**. The F1 and F6 structure, recognized as major structures by earlier researchers, represents the horst block that acts as a structural boundary, defining the elevation disparities between the Southern Mountains, the Baturagung Range, and the Yogyakarta depression. This structural element plays a critical role in delineating the geological configuration of the region, as it separates distinct topographical and geological domains (Rahardjo et al., 1995). The structures of F1 and F5 have similar directions Opak Faults by previous researchers (Pena-Castellnou et al., 2021). In our study area, based on a previous study with a geomorphological method (Pena-Castellnou et al., 2021), there is a geomorphological phenomenon known as triangular facets. Triangular facets are unique triangular-shaped landforms closely linked to normal faulting. They form as a result of differential erosion or weathering along fault scarps, where one side of the fault is uplifted, and the other side is down-dropped (Leeder and Jackson, 1993; Jackson and Leeder, 1994).

We utilized additional data points from Saputra et al. (2018) to obtain the distribution of strikes and dips in the study area. Two significant NE-SW-oriented structures characterize the northern segment **(Fig. 8)**. On the western side, we find the F3 fault, which aligns with previous interpretations (Rahardjo et al., 1995 in **Fig. 2**; Natawidjaja, 2007), while on the eastern side, the boundary is defined by the F1 fault. Moving southward, the F4 fault, with an E-W orientation, marks the southern limit of this segment. A distinctive shield-shaped hill commands attention within this region, bor-

Fig. 8. Triangular facets observed on the hillslope located in the northwest of the Baturagung Range showing F1 and F5 faults as major controller of study area (modified from Pena-Castellnou et al., 2021).

Фиг. 8. Наблюдаемые треугольные фасеты на склоне холма, расположенные на северо-западе хребта Батурагунг, показывающие разломы F1 и F5 как основные контролирующие элементы исследуемой области (изменено по Pena-Castellnou и др., 2021).

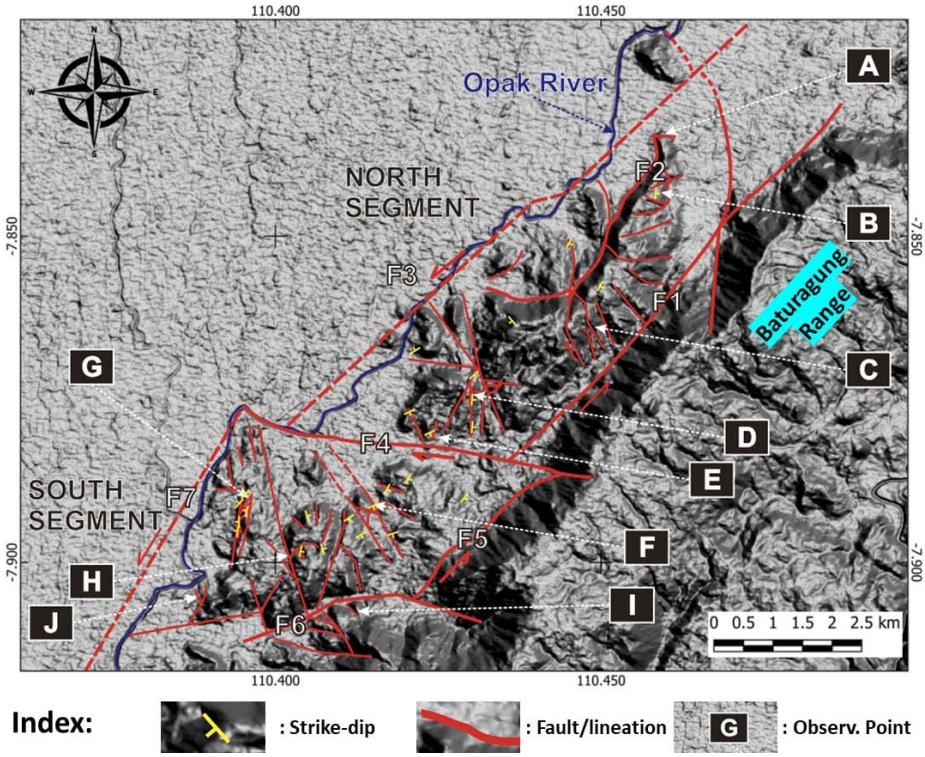

Fig. 9. The morphotectonic map of the study area, including observation points and strike-dip data, reveals clear distinctions between the northern and southern segments.

Фиг. 9. Морфотектоническая карта исследовательской области, включающая наблюдательные пункты и данные о страйк-дипе, показывает явные различия между северным и южным сегментами.

dered by the F2 structure to the west. This hill predominantly extends in an NE-SW direction, with the layers of the Semilir Formation on the hill dipping toward the southeast. Notably, minor structures on this hill exhibit diverse orientations, ranging from NE-SW to NW-SE. To the west of this shield-shaped hill, smaller hills with southeastward-dipping layers are aligned parallel to their eastern counterparts. The shield-shaped hill has experienced an inversion phase, supported by the presence of a high-angle reverse fault (75°) at observation point A. This high-angle fault is a distinct indicator of tectonic inversion in the area.

To the south of this shield-shaped hill, various linear structures radiate in different directions, including N-S, NW-SE, W-E, and NE-SW. A sinistral strike-slip fault structure is evident in the southernmost area, specifically at observation point D. This structure correlates with a high-angle reverse fault (64°) in the western section, as observed at point D1 **(Fig. 6b)** signifying tectonic inversion in this region. The diverse orientations of rock layers within this area include W-E, NE-SW, N-S, and NE-SW strikes, underscoring the significant influence of fault structures on the geological setting.

This area exhibits linear features with varying orientations in the southern segment **(Fig. 9)**. The F5 structure bounds it to the east, adjacent to the Baturagung Range. To the north, it is delineated by the F4 structure, while to the south, it is defined by the F6 structure. To the east, it is bounded by the parallel F7 structure, following the course of the Opak River. Within the southern segment, the orientation of the Semilir Formation layers is opposite. Specifically, to the west, around observation point G, the layers dip to the west, while around observation point H, they dip to the east. Previous researchers (Saputra et al., 2018) interpreted this area as a fold. However, due to the brittleness of the Semilir Formation, we have interpreted this phenomenon as primarily resulting from fault structure movements.

Around observation point G, linear structures have a dominant orientation, almost N-S to NW-SE. The NW-SE-oriented linear structure extends significantly from the F4 fault to the F6 fault. This structure is almost parallel to the one found at observation point F, which has an NW-SE orientation. Near observation point H, in addition to the NW-SE oriented linear structures, there are minor structures with varying orientations, ranging from NE-SW to NW-SE.

The F1, F3, F4, F5, F6, and F7 **(Fig. 10)** generally present transpressive horst minor faults inside the zone.

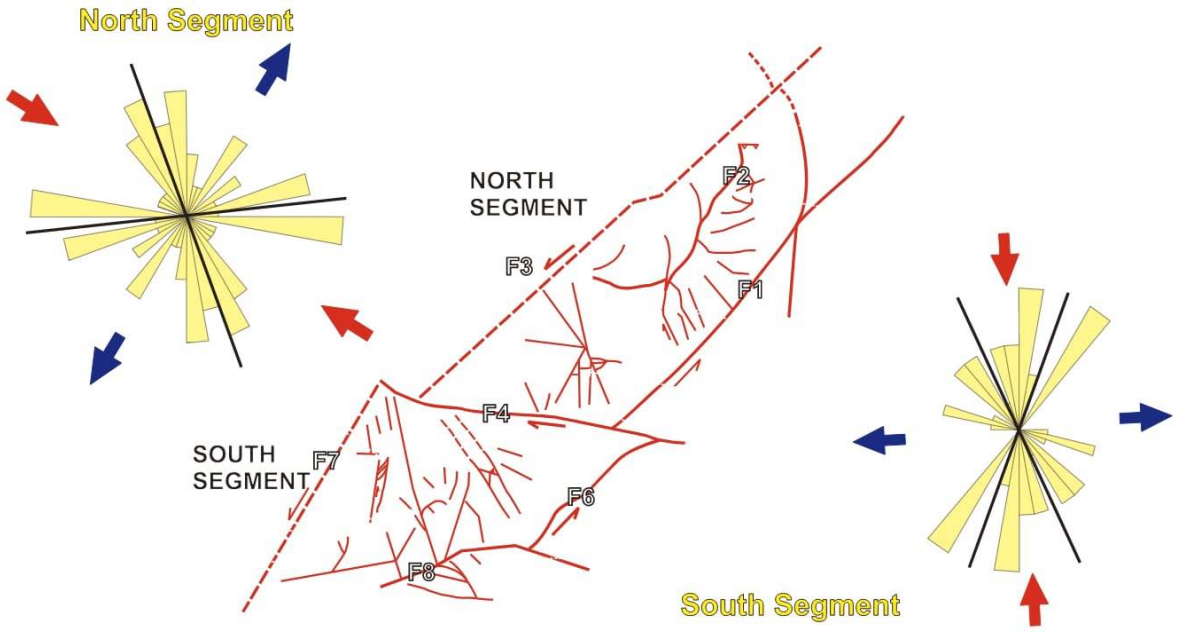

Fig. 10. Rossette's diagram shows the disparities between the northern and southern segments.

Фиг. 10. Диаграмма розетки показывает различия между северным и южным сегментами.

Near these major faults, secondary faults and fractures can be correlated with either localized effects at specific fault locations. According to McGrath and Davison (1995), the observed variance in damage zone geometries in strike-slip faults is mostly due to distinct stress regimes, namely transpression, transtension, and simple shear. Strain is often partitioned in transpressional settings into strike-slip motion along a main fault system and shortening perpendicular to the strike-slip fault (Cowgill et al., 2004).

Our rosette diagram analysis results further substantiate the disparities between the northern and southern segments. We systematically translated the structures and lineations from both the northern and southern segments into rosette diagrams **(Fig. 10)**. These graphical representations enable us to deduce the distinct tectonic characteristics of each segment. Within the northern segment, the rosette diagram distinctly illustrates a main compression direction extending from NW-SE, concurrently with a tensional direction spanning from NE-SW. In contrast, the southern segment exhibits a markedly different pattern, characterized by a main compression direction from N-S and an associated tensional direction extending from W-E.

CONCLUSION

We conclude that integrating UAV photogrammetry and Digital Elevation Model (DEM) data has significantly enhanced our understanding of the geological structures within the Semilir Formation in the Opak Fault Zone. Utilizing this method on the brittle Semilir Formation allows for a sufficiently accurate depiction during geological structural interpretation.

Several significant conclusions emerge from the results of structural geology interpretation. Firstly, the study area is divided into two distinct segments, the North and South segments, each characterized by varying morphological formations. In the North Segment, elongated hills aligned in an NE-SW direction resembling the Opak Fault are evident, while the South Segment displays a relatively North-South block lineation. Secondly, different structural characteristics are observed within each segment, including fault orientations and associated geological features. UAV-based aerial interpretation in the North Segment reveals major faults and minor shear structures, indicating a complex fault system controlling hill morphology, supported by geological field surveys confirming the presence of reverse faults and sinistral strike-slip faults. The South Segment exhibits significant structural heterogeneity with NW-SE oriented faults and en-echelon fractures, suggesting transpressive features, alongside notable N-S oriented structural lineations indicating complex fault systems.

Furthermore, morphotectonic analysis highlights the influence of fault-related activities and tectonic inversion processes, with major fault lines delineating structural boundaries and confirming distinct tectonic characteristics between the northern and southern

segments. Based on the rosette diagram, the main compression in the north segment extends from NW-SE, while in the south segment, it extends from N-S. The analysis identifies the study area as a reactivation zone of the Opak fault, indicated by the presence of high-angle reverse faults. This reactivation zone is interpreted as a zone of destruction resulting from Opak fault movement, previously identified as a sinistral strike-slip fault.

In conclusion, the integrated approach combining UAV-based analysis, geological field surveys, and morphotectonic mapping offers valuable insights into the complex tectonic processes and fault systems shaping the landscape of the study area.

REFERENCES

Abidin, H. Z., Andreas, H., Kato, T., Ito, T., Meilano, I., Kimata, F., Natawidjaya, D. H., and Harjono, H. (2009a). Crustal deformation studies in Java (Indonesia) using GPS. J. Earthq. Tsunami, 3, 77–88. DOI:10.1142/S1793431109000445

Abidin, H. Z., Andreas, H., Meilano, I., Gamal, M., Gumilar, I., and Abdullah, C. I. (2009b). Seismic deformation and post-seismic deformation of the 2006 Yogyakarta earthquake from GPS survey results. Jurnal Geologi Indonesia, 4, 275–284.

Beauchamp, W., Allmendinger, R., Barazangi, M., Demnati, A., El Alji, M., and Dahmani, M. (1999). Inversion tectonics and the evolution of the High Atlas Mountains, Morocco, based on a geological-geophysical transect. Tectonics, 18, 163–184. doi:10.1029/1998TC900015

Beauchamp, W., Barazangi, M., Demnati, A., and El Alji, M. (1996). Intracontinental rifting and inversion: Missour Basin and Atlas Mountains, Morocco. American Association of Petroleum Geologists Bulletin, 80, 1459–1482.

Consultative Group on Indonesia. (2006). Preliminary damage and loss assessment, Yogyakarta and central Java natural disaster: A joint report of BAPPENAS, the provincial and local governments of D.I. Yogyakarta, the provincial and local governments of central Java, and international partners. In The 15th Meeting of the Consultative Group on Indonesia (CGI), Jakarta, June 14, 2006. Jakarta.

Corradetti, A., Seers, T., Mercuri, M., Calligaris, C., Busetti, A., and Zini, L. (2022). Benchmarking Different SfM-MVS Photogrammetric and iOS LiDAR Acquisition Methods for the Digital Preservation of a Short-Lived Excavation: A Case Study from an Area of Sinkhole Related Subsidence. Remote Sensing, 14(20). doi:10.3390/rs14205187.

Cowgill, E., Yin, A., Arrowsmith, J.R., Wang, X.F., & Zhang, S. (2004). The Akato Tagh bend along the Altyn Tagh fault, NW Tibet 1, Cenozoic structure, smoothing by vertical-axis rotation, and the effect of topographic stresses on borderland faulting. Geological Society of America Bulletin, 116, 1423-1442.

Cruikshank, K. M., Zhao, G., and Johnson, A. M. (1991). Duplex structures connecting fault segments in Entrada Sandstone. Journal of Structural Geology, 13, 1185-1196.

Fossen, H., and Hesthammer, J. (1997). Geometric analysis and scaling relations of deformation bands in porous sandstone. Journal of Structural Geology, 19, 1479-1493.

Fukuoka, K., Ehara, S., Fujimitsu, Y., Udi, H., Setyawan, A., Setyadji, L. D., Harijoko, A., Pramumijoyo, S., Setiadi, Y., and Wahyudi. (2006). Interpretation of the 27 May 2006 Yogyakarta Earthquake Hypocenter and Subsurface Structure Deduced from the Aftershock and Gravity data. In The Yogyakarta Earthquake of May, 27. Star Publisher, Los Angeles.

Geology of Yogyakarta, Java: The dynamic volcanic arc city. The Geological Society of London, IAEG 2006 Paper number 363, 1-7.

Gomez, F., Beauchamp, W., and Barazangi, M. (2000). Role of the Atlas Mountains (northwest Africa) within the African-Eurasian plate-boundary zone. Geology, 28, 775-778. doi:10.1130/0091-7613(2000)28<775:ROTAMN>2.0.CO;2

Hall, R. (2012). Late Jurassic-Cenozoic reconstructions of the Indonesian region and the Indian Ocean. Tectonophysics, 570-571, 1-41. https://doi.org/10.1016/j.tecto.2012.04.021

Hamilton, W. (1979). Tectonics of the Indonesian Region. USGS Professional Paper. United States Printing Office, Washington. https://doi.org/10.3133/pp1078

Hill, K. C., Keetley, J. T., Kendrick, R. D., and Sutriyono, E. (2004). Structure and hydrocarbon potential of the New Guinea fold belt. In K. R. McClay (Ed.), Thrust Tectonics and Hydrocarbon Systems (pp. 494-514). American Association of Petroleum Geologists Memoir 82.

Hodgetts, D., Drinkwater, N. J., Hodgson, D., Kavanagh, J., Flint, S., Keogh, K. J., Howell, J. (2004). Three-dimensional geological models from outcrop data using digital data collection techniques: an example from the Tanqua Karoo depocentre, South Africa. In A. Curtis and R. Wood (Eds.), Geological Prior Information. Geological Society Special Publication 239, 57-75.

Jackson, J., & Leeder, M. (1994). Drainage systems and the development of normal faults – an example from Pleasant Valley, Nevada. Journal of Structural Geology, 16, 1041–1059.

James, M.R., Robson, S., 2014. Mitigating systematic error in topographic models derived from UAV and ground-based image networks. Earth Surf. Process. Landforms 39 (10), 1413–1420. https://doi.org/10.1002/esp.3609.

Karnawati, D., Pramumijoyo, S., and Hendrayana, H. (2006).

Keller, E.A. and Pinter, N. (1996) Active Tectonics: Earthquakes, Uplift, and Landscape. Prentice Hall.

Kim, Y. S., Peacock, D. C. P., and Sanderson, D. J. (2004). Fault damage zones. Journal of Structural Geology, 26(3), 503–517. doi:10.1016/j.jsg.2003.08.002

Konstantinovskaya, E. A., Harris, L. B., Poulin, J., and Ivanov, G. M. (2007). Transfer zones and fault reactivation in inverted rift basins: Insights from physical modeling. Tectonophysics, 441, 1-26. doi:10.1016/j.tecto.2007.06.002

Koulakov, I., et al., 2007. P and S velocity structure of the crust and the upper mantle beneath central java from local tomography inversion, J. geophys. Res., 112, B08310.

Leeder, M.R., & Jackson, J.A. (1993). The interaction between normal faulting and drainage in active extensional basins, with examples from the western United States and central Greece. Basin Research, 5(2), 9–102.

Li J., Ding W., Lin J., Xu Y., Kong F., Li S., Huang X., Zhou Z. (2021) Dynamic processes of the curved sub-

duction system in Southeast Asia: A review and future perspective. Earth-Science Rev., 217, 103647. https://doi.org/10.1016/j.earscirev.2021.103647

Manna, L., Perozzo, M., Menegoni, N., Tamburelli, S., Crispini, L., Federico, L., Seno, S., and Maino, M. (2023). Anatomy of a km-scale fault zone controlling the Oligo-Miocene bending of the Ligurian Alps (NW Italy): integration of field and 3D high-resolution digital outcrop model data. Swiss Journal of Geosciences, 1-29. doi:10.1186/s00015-023-00444-1

McCaffrey, K.J.W., Jones, R.R., Holdsworth, R.E., Wilson, R.W., Clegg, P., Imber, J., Holliman, N., Trinks, I. (2005). Unlocking the spatial dimension: digital technologies and the future of geosciences fieldwork. Journal of the Geological Society of London, 162, 927-938.

McGrath, A.G., and Davison, I. (1995). Damage zone geometry around fault tips. Journal of Structural Geology, 17, 1011-1024.

Menegoni, N., Inama, R., Crozi, M., and Perotti, C. (2022). Early deformation structures connected to the progradation of a carbonate platform: The case of the Nuvolau Cassian platform (Dolomites - Italy). Marine and Petroleum Geology, 138. https://doi.org/10.1016/j.marpetgeo.2022.105574

Menegoni, N., Maino, M., Toscani, G., Mordeglia, L. I., Valle, G., and Perotti, C. (2023). Holocene Deformations at the Po Plain – Southern Alps Transition (Lake Maggiore, Italy): Inferences on Glacially vs. Tectonic-Induced Origin. Geosciences, 13(286). https://doi.org/10.1016/j.marpetgeo.2022.105574

Metcalfe I. (2017) Tectonic evolution of Sundaland. Bull. Geol. Soc. Malaysia, 63, 27-60. https://doi.org/10.7186/bgsm63201702

Natawidjaja, D. H., and Daryono, M. R. (2016). Present-day tectonics and earthquake history of Java, Indonesia. In Proceedings GEOSEA XIV Congress and 45th IAGI Annual Convention 2016.

Natawidjaja, D.H. (2007). Tectonic Setting of Indonesia and Modeling of Earthquake and Tsunami Sources. Training in Tsunami Run-up Modeling. Ministry of Research, Technology and Higher Education of the Republic of Indonesia: Jakarta, Indonesia.

Ollier, C.D. (1981). Tectonics and Landforms. Longman, London, p. 324.

Panara, Y., Menegoni, N., Carboni, F., and Inama, R. (2022). 3D digital outcrop model-based analysis of fracture network along the seismogenic Mt. Vettore Fault System (Central Italy): The importance of inherited fractures. Journal of Structural Geology, 161. https://doi.org/10.1016/j.jsg.2022.104654

Pena-Castellnou, S., Steinritz, V., Marliyani, G. I., and Reicherter, K. (2021). Active tectonics of the Yogyakarta area (Central Java, Indonesia): Preliminary findings obtained from a tectonic-geomorphic evaluation. IOP Conference Series: Earth and Environmental Science, 851(1). https://doi.org/10.1088/1755-1315/851/1/012005

Pringle, J.K., Westerman, A.R., Clark, J.D., Drinkwater, N.J., Gardiner, A.R. (2004). 3D high-resolution digital models of outcrop analogue study sites to constrain reservoir model uncertainty: an example from Alport Castles, Derbyshire, UK. Petroleum Geoscience, 10, 343-352. https://doi.org/10.1144/1354-079303-617

PUSGEN. (2017). Map of the source and hazard of the Indonesian earthquake year. Center for Research and Development of Housing and Settlements, Research and Development Agency, Ministry of Public Works and Housing.

Rahardjo, W., Sukandarrumidi, and H. Rosidi (1995). Geologic map of the Yogyakarta quadrangle, Java, scale 1:100,000, 8 pp. Geology Survey Indonesia, Ministry of Mines, Jakarta.

Sagir, A. (2001). Ancient deep faults, their reactivation and peculiarities under different geodynamic conditions in eastern Yakutia (northeast Russia). Polarforschung, 69, 117–184.

Saputra A., Gomez C., Delikostidis I., Zawar-Reza P., Hadmoko D.S., Sartohadi J., Setiawan M.A. (2018) Determining Earthquake Susceptible Areas Southeast of Yogyakarta, Indonesia–Outcrop Analysis from Structure from Motion (SfM) and Geographic Information System (GIS). Geosciences. 8(4):2076–3263. https://doi.org/10.3390/geosciences8040132

Schoenbohm, L., Whipple, K., Burchfiel, B., and Chen, L. (2004). Geomorphic constraints on surface uplift, exhumation, and plateau growth in the Red River region, Yunnan Province, China. Geological Society of America Bulletin, 116, 895–909. https://doi.org/10.1130/b25364.1.

Sibson, R. H. (1985). A note on fault reactivation. Journal of Structural Geology, 7(6), 751–754. https://doi.org/10.1016/0191-8141(85)90150-6

Silva, P. G., Goy, J. L., Zazo, C., and Bardajm, T. (2003). Fault-generated mountain fronts in Southeast Spain: geomorphologic assessment of tectonic and earthquake activity. Geomorphology, 250, 203–226.

Smith, S. A. F., Tesei, T., Scott, J. M., & Collettini, C. (2017). Reactivation of normal faults as high-angle reverse faults due to low frictional strength: Experimental data from the Moonlight Fault Zone, New Zealand. Journal of Structural Geology, 105(July), 34–43. https://doi.org/10.1016/j.jsg.2017.10.009

Snyder, N.P., Whipple, K.X., Tucker, G.E., and Merritts, D.J. (2000). Landscape response to tectonic forcing: Digital elevation model analysis of stream profiles in the Mendocino triple junction region, northern California. Geological Society of America Bulletin, 112, 1250–1263. https://doi.org/10.1130/0016-7606(2000)112<1250:lrttfd>2.0.co;2.

Stewart, I. S., and Hancock, P. L. (1990). What is a fault scarp? Episodes, 13, 256–263.

Stewart, I. S., and Hancock, P. L. (1994). Neotectonics. In: Hancock, P. L. (Ed.), Continental Deformation. Pergamon, Oxford, pp. 370–409.

Surono, B., Toha, and I. Sudarno (1992). Geological map of Surakarta and Giritontro quadrangle sheet number 1408-3 and 1407-6, scale 1:100,000. Center for Geological Research and Development Bandung.

Surono. (2008). Sedimentation of the Semilir Formation in Sendang Village, Wuryantoro, Wonogiri, Central Java. Journal of Geological Resources, 18(1), 29-41.

Tannant, D. D., Giordan, D., and Morgenroth, J. (2017). Characterization and analysis of a translational rockslide on a stepped-planar slip surface. Engineering Geology, 220, 144–151. https://doi.org/10.1016/j.enggeo.2017.02.004

Tsuji, T., Yamamoto, K., Matsuoka, T., Yamada, Y., Onishi, K., Bahar, A., Meilano, I., and Abidin, H. Z. (2009). Earthquake fault of the 26 May 2006 Yogyakarta earthquake observed by SAR interferometry. In Earth Planets Space, 61.

Turner, J. P., and Williams, G. A. (2004). Sedimentary basin

inversion and intra-plate shortening. Earth-Science Reviews, 65, 277–304.

USGS Preliminary Earthquake Report, The website of United States Geological Survey, Earthquake Hazards Program, (available at http://earthquake.usgs.gov/eqcenter/eqinthenews /2006/usneb6/), 2006.

Vollgger, S. A., and Cruden, A. R. (2016). Mapping folds and fractures in basement and cover rocks using UAV photogrammetry, Cape Liptrap and Cape Paterson, Victoria, Australia. Journal of Structural Geology, 85, 168–187. https://doi.org/10.1016/j.jsg.2016.02.012

Wagner, D., Koulakov, I., Rabbel, W., Luehr, B. G., Wittwer, A., Kopp, H., Bohm, M., & Asch, G. (2007). Joint inversion of active and passive seismic data in Central Java. Geophysical Journal International, 170(2), 923–932. https://doi.org/10.1111/j.1365-246X.2007.03435.x

Walter, T. R., Wang, R., Luhr, B. G., Wassermann, J., Behr, Y., Parolai, S., Anggraini, A., Günther, E., Sobiesiak, M., Grosser, H., Wetzel, H. U., Milkereit, C., Sri Brotopuspito, P. J. K., Harjadi, P., and Zschau, J. (2008). The 26 May 2006 magnitude 6.4 Yogyakarta earthquake south of Mt. Merapi volcano: Did lahar deposits amplify ground shaking and thus lead to the disaster? Geochemistry, Geophysics, Geosystems, 9(5). https://doi.org/10.1029/2007GC001810

Withjack, M. O., Olsen, P. E., and Schlishe, R. W. (1995). Tectonic evolution of the Fundy rift basin, Canada: Evidence of extension and shortening during passive margin development. Tectonics, 14, 390–405. https://doi.org/10.1029/94TC03087.